1   *Systematic Optimization Approach for the Efficient Management of the Photo-*

2   *Fenton Treatment Process*

3   *Francesca Audino*; Gerard Campanya; Moisès Graells; Antonio Espuña; Montserrat Pérez-*

4   *Moya.* Chemical Engineering Department, Universitat Politècnica de Catalunya. Escola

5   d'Enginyeria de Barcelona Est (EEBE), Av. Eduard Maristany, 10-14, 08019, Barcelona, Spain.

6   **francesca.audino@upc.edu*

7   *gcampanya@gmail.com*

8   *moises.graells@upc.edu*

9   *antonio.espuna@upc.edu*

10   montserrat.perez-moya@upc.edu

11   **coresponding author:* Francesca Audino

12   **ABSTRACT**

13   The photo-Fenton process is a photochemical process that has proved to be highly efficient in

14   degrading new potentially harmful contaminants. Despite of this, scarce attention has been paid

15   to the development of systematic procedures and optimisation strategies to efficiently operate

16   such a process. The present work aims at investigating the effectiveness of a model-based

17   approach in carrying out the dynamic optimisation of the recipe of a photo-Fenton process,

18   performed in fed-batch mode (reactant dosage).

19   This work addressed and solved multiple optimisation problems, searching for the optimal

20   hydrogen peroxide (H_2O_2) dosage profile, and Pareto frontiers were built accordingly in order to

21   point out the interaction between three main process efficiency parameters, such as the

22   processing time, the total amount of H_2O_2 used, and the Total Organic Carbon (TOC) reduction.

23   Such a study allows mapping the best operating conditions and provides a practical decision-

24   making oriented overview of the process. An economic study was also carried out with the aim

25   of finding out the optimal H_2O_2 dosage profile that guarantees the minimum operating cost

26   under a varying set of operational and environmental constraints, such as the TOC reduction. A

27   semi-empirical kinetic (shortcut model) was adopted and properly adapted in order to describe

28   the evolution of the system under a flexible reactant dosage, and the subsequent dynamic

29   optimisation problem was addressed applying a direct simultaneous optimisation method.

30   Results have been presented and discussed in regard of optimal H_2O_2 dosage under a variety of

31 objectives and constraints, both economic and environmental. This allows concluding that a

32 model-based optimisation approach would provide further operational insight and practical

33 recipe adjustment in a fast and reliable way, with reduced experimental work and decision-

34 making focus.

35

36 **Keywords: AOPs, photo-Fenton, H_2O_2 dosage, dynamic optimisation, Pareto frontiers,**

37 **decision-making.**

38

39

40 **Acronyms**

41

H_2O_2	Hydrogen peroxide
Fe^{2+}	Ferrous ion
Fe^{3+}	Ferric ion
R	Free radicals
M	Organic matter
MX_1	Partially oxidized organic: first intermediate
MX_2	Partially oxidized organic: second intermediate
DO	Dissolved oxygen
DO^*	Dissolved oxygen concentration saturation
TOC	Total organic carbon

42

43

44 **Nomenclature**

45

F(t)	Inlet flow-rate	L h^{-1}
$f_i(t)$	Molar inlet flow-rate for each component i	mmol h^{-1}
V	Total volume of the reactor	L
$F(t)/V$	Dilution factor	adimensional
I	Irradiance	W m^{-2}
$[C_i]^{IN}$	Concentration of component i in the inlet flow	mM
$[C_i]$	Concentration of component i inside the reactor	mM
$[C_i]^0$	Initial concentration of component i inside the reactor	mM
t	Time	h
τ	Final reaction time (reaction span)	h
$\chi(t)$	TOC removal at a generic time t	adimensional
$\chi(\tau)$	Final TOC removal (at τ)	adimensional

A(t)	Amount of H_2O_2 employed at a generic time t	mmol
$A(\tau)$	Total amount of H_2O_2	mmol
k_j	Kinetic constants for each reaction j	Several units
r_i	Reaction rates for each component i	mmol h^{-1}
$g1_{DO}$, $g2_{DO}$, $c1_{DO}$	Stoichiometric coefficients in the dissolved oxygen balance	Several units
kla	Gas–liquid mass transfer coefficient in the dissolved oxygen balance	h^{-1}
$C_{N, N=1,2,3}$	Unit cost coefficients	Several units

46

47

48 **1. INTRODUCTION**

49

50 In the last years, the research, development and implementation of Advanced Oxidation

51 Processes (AOPs), both for industrial and urban wastewaters, have received considerable

52 attention. AOPs have emerged as the only feasible option for the treatment of hardly

53 biodegradable or toxic substances that can resist or damage conventional biological treatments

54 [Oller et al. (2011)] and for the treatment of the so-called Contaminants of Emerging Concern

55 (CECs). CECs are a group of chemicals that are being detected in waters in very low

56 concentrations (ng L^{-1} and µg L^{-1}) thanks to new and more powerful analytical techniques, and

57 that may be included in future environmental regulations depending on the results of the

58 investigations on their effects on human health and the environment.

59

60 Directive 2013/39/EU of the European Parliament and of the Council of 12 August 2013

61 amending Directives 2000/60/EC and 2008/105/EC as regards priority substances in the field of

62 water policy, states the importance of CECs monitoring and updates the list of priority

63 substances. According to the European Commission, another important goal will also be the

64 reinforcement of the risk assessment of pharmaceutical products [Ribeiro et al. (2015)].

65

66 Although AOPs are considered clean technologies for this challenge, they are also expensive

67 because of the consumption of energy and chemical reagents, which increases with treatment

68 time. Hence, the achievement of a practical application of AOPs is required. Towards this end,

69 the key issue is the achievement of design and operation approaches providing optimal

70 economic and environmental performance of AOPs.

71

72 Specifically, the present study focuses on operation of the photo-Fenton process, which is of

73 added interest among the AOPs, since it has proved to be highly efficient for the removal of

74 CECs [Miralles-Cuevas et al. (2014)], and for the possibility to exploit solar light. The photo-

75 Fenton process is a photochemical process based on the Fenton reaction between the ferrous

76 iron Fe^{2+}, that is the catalyst, and the hydrogen peroxide H_2O_2, such as the oxidant, that leads

77 to the formation of hydroxyl radicals $^{\cdot}OH$, the active oxidizing species having an oxidation

78 potential (2.8V) much higher than other traditional oxidants.

79

80 In the last decade, a remarkable experimental effort has been made to better understand the

81 photo-Fenton process as a whole [Andreozzi et al. (2000), Farias et al. (2007)]. As pointed out

82 in a review by Pignatello et al. (2006), several studies performed at laboratory scale have

83 investigated the role of H_2O_2 consumption, the processing time and the mineralization rate,

84 being key process efficiency parameters that affect the overall kinetics. Subsequently, Zapata et

85 al. (2010) published an important study, also performed at laboratory scale, and evaluating the

86 effect of temperature, dissolved iron concentration, and dissolved organic carbon (DOC) as well

87 as their relationship to such key process efficiency parameters.

88

89 Conversely, only few studies [Moreno-Benito et al. (2013)] have adopted a model-based

90 approach for determining the best operating conditions that can help the development of

91 practical applications.

92

93   In the optimisation of the batch wise operation of photo-Fenton processes, the hydrogen

94   peroxide dosage strategy plays a crucial role. Experimental results have highlighted the

95   activation of inefficient reactions scavenging hydrogen peroxide, the most expensive process

96   reactant, which can be avoided or reduced by proposing a proper flexible recipe with gradual

97   dosage [Yamal-Turbay et al. (2013), (2012)].

98

99   According to the literature survey, up until now, the determination of an efficient H_2O_2 dosage

100   profile has been faced mostly following an experimental approach [Prieto-Rodríguez et al.

101   (2011)] based on manual H_2O_2 dosing that has led to low process performance or, for control

102   purposes [Ortega-Gómez et al. (2012)]. Hence, a greater effort is needed in regard of

103   optimisation strategies, whose success also depends on the availability of reliable and

104   computationally affordable models.

105

106   With regard to photo-Fenton kinetics modelling, two main approaches can be found in literature,

107   such as empirical models [Kusic et al. (2006), Pérez-Moya et al. (2008)] that cannot be scaled

108   up and do not address the process dynamics, and First Principles Models (FPMs) [Jeong et al.

109   (2005), Conte et al. (2012)] that are unaffordable even for very simple molecules.

110

111   Therefore, a compromise solution was adopted such as a semi-empirical kinetic (shortcut)

112   model based on simplified photo-Fenton reactions and lumped parameters (for parent

113   compound, intermediates and free radicals). This model was properly adapted to investigate the

114   effectiveness, efficiency and reliability of a model-based approach in:

115

116   i)   Investigating the interrelations between the main variables that affect the process

117   efficiency, such as the processing time, the total amount of hydrogen peroxide and

118   the final Total Organic Carbon (TOC) reduction. Such analysis allows aiding the

119   decision making by providing an overview of the best operating conditions, e.g. in

120   terms of total amount of H_2O_2 and processing time to achieve a predetermined final

121   TOC reduction.

122   ii)   Performing the dynamic optimisation of the H_2O_2 dosage profile to drive the process

123   at the minimum processing cost while ensuring operational and environmental

124   constraints such as TOC removal.

125

126   For this problem, a multi-objective optimisation (MO) strategy has been proposed and Pareto

127   frontiers have been built accordingly. By building the Pareto frontier, several optimal operating

128   conditions for different treatment configurations can be easily and quickly identified. Besides,

129   unfeasible operating conditions and unattainable process performances are also recognized

130   and duly mapped.

131

132   Moreover, the proposed systematic approach offers promising opportunities for the selection of

133   the best treatment option in a fast and reliable way. The best treatment option, or rather the one

134   that allows meeting the quality standards at the most convenient cost, can consist of several

135   conventional and/or alternative processes, e.g. combination of biological processes and AOPs.

136   According to the strategy proposed by Oller et al. (2011), when considering the possibility to

137   combine biological processes with the AOPs, the optimal operating conditions for the combined

138   process are needed. However, this requires the optimisation of each single chemical and

139   biological step. Thus, the proposed procedure fulfils a prerequisite needed for efficiently

140   selecting the best operating conditions in terms of both water quality (TOC reduction) and

141   relative treatment cost (total amount of hydrogen peroxide and treatment time).

142

143

144   **2. METHODOLOGICAL FRAMEWORK AND TOOLS**

145

146   As highlighted in *Fig.1*, the proposed methodology consists of four different steps, such as the

147   kinetic and reactor modelling and the dynamic simulation and optimisation that will be analysed

148   in detail in the following sections.

149

150   **Fig.1** Scheme of the proposed methodology consisting of four specific steps: the kinetic

151   modelling, the reactor modelling, the dynamic simulation and the dynamic optimisation

152

153   **2.1 *KINETIC MODEL AND DATA***

154

155   The shortcut model by Cabrera Reina et al. (2012), relying on simplified photo-Fenton process

156   reactions for the prediction of Total Organic Carbon [TOC], hydrogen peroxide [H_2O_2] and

157   dissolved oxygen [DO] concentration evolution, was selected. This model is proposed and fit for

158   paracetamol (PCT) as model pollutant and assumes nine processes and eight states (the

159   ferrous and ferric iron Fe^{2+} and Fe^{3+}, the hydrogen peroxide H_2O_2, the free radicals R, the

160   dissolved oxygen DO, the parent compound M and two partially oxidized organics, such as MX_1

161   and MX_2). The data and parameter values reported [Cabrera Reina et al. (2012)] were also

162   assumed.

163

164

165   **Fig.2** Kinetic mechanism proposed by Cabrera Reina et al. (2012)

166

167   Such model was selected since it represents an interesting compromise between the complexity

168   of the detailed First Principle Models [Jeong et al. (2005), Conte et al. (2012)] that can ensure

169   rigorousness but at the expense of computational time and the oversimplification of Empirical

170   Models [Kusic et al. (2006), Pérez-Moya et al. (2008)] based on surface response that do not

171   provide information about the process dynamics.

172

173   The model also allows taking into account the hydrogen peroxide optimisation since it accounts

174   for the inefficient reactions involving H_2O_2 and the free radicals (reactions 3 and 4 in *Fig.2*) that

175   lead to an inefficient use of the oxidant, highlighted by an increase in the dissolved oxygen

176   concentration. Increasing the hydrogen peroxide concentration reduces the process efficiency

177   since it increases the concentration of radicals [R]. Increasing [R] increases both the rate of

178   oxidation of organic matter and the rate of inefficient production of DO; the latter being more

179   sensitive to [R]. This is modelled by first order (linear, $\propto [R]$) efficient reactions and second

180   order (quadratic, $\propto [R]^2$) inefficient reactions, which rate is favoured by the excess of radicals.

181   The model grasps this trade-off and reveals the subsequent optimisation opportunities.

182

183 The use of lumped parameters (for parent compound, M, and resulting intermediates, MX_1 and

184 MX_2, as well as for free radicals, R) is also very functional and allows focusing on those easily

185 measurable factors (TOC and DO concentrations, monitored by apposite sensors), which

186 facilitate the development of real-world applications.

187

188

189 **2.2 REACTOR MODEL: H_2O_2 DOSAGE**

190

191 A reactor model was proposed to consider the H_2O_2 dosage. It is given by a set of Ordinary

192 Differential Equations (ODEs), (*Eqs. (1) - (10)*), describing the mass balances into the fed batch

193 reactor, such as when a reactant dosage is performed:

194

$$\frac{dV}{dt} = F(t) \tag{1}$$

$$\frac{d[H_2O_2]}{dt} = \frac{F(t)}{V} \times ([H_2O_2]^{IN} - [H_2O_2]) - r1 - r3 \tag{2}$$

$$\frac{d[Fe^{2+}]}{dt} = \frac{F(t)}{V} \times ([Fe^{2+}]^{IN} - [Fe^{2+}]) - r1 - r2 \tag{3}$$

$$\frac{d[Fe^{3+}]}{dt} = \frac{F(t)}{V} \times ([Fe^{3+}]^{IN} - [Fe^{3+}]) + r1 + r2 \tag{4}$$

$$\frac{d[R]}{dt} = \frac{F(t)}{V} \times ([R]^{IN} - [R]) + r1 + r2 - r3 - (2 \times r4) - r5 - r6 - r7 - r8 - r9 \tag{5}$$

$$\frac{d[M]}{dt} = \frac{F(t)}{V} \times ([M]^{IN} - [M]) - r5 - r6 \tag{6}$$

$$\frac{d[MX_1]}{dt} = \frac{F(t)}{V} \times ([MX_1]^{IN} - [MX_1]) + r5 + r6 - r7 - r8 \tag{7}$$

$$\frac{d[MX_2]}{dt} = \frac{F(t)}{V} \times ([MX_2]^{IN} - [MX_2]) + r7 + r9 \tag{8}$$

$$\frac{d[DO]}{dt} = \frac{F(t)}{V} \times ([DO]^0 - [DO]) + (g1_{DO} \times r3) + (g2_{DO} \times r4) - (c1_{DO} \times r5) \tag{9}$$
$$+ (K_{La} \times ([DO]^* - [DO]))$$

$$\frac{d[TOC]}{dt} = \frac{d[M]}{dt} + \frac{d[MX_1]}{dt} + \frac{d[MX_2]}{dt} \tag{10}$$

195

196   In the equations above, $F(t)$, represents the inlet flow-rate (L h^{-1}) that produces a variation in

197   the total volume of the reactor V (L), while $F(t)/V$ represents the dilution factor due to the

198   continuous addition of the hydrogen peroxide solution during the reaction time.

199

200   The symbols $[C_i]^{IN}$ and $[C_i]$ refer to the concentrations (mM) in the inlet flow-rate and inside the

201   reactor, respectively, for each component. Since the study just considers the hydrogen

202   peroxide dosification, only $[H_2O_2]^{IN}$ is different from zero, while the rest of inlet concentrations

203   are null. Finally, $[DO]^*$ represents the dissolved oxygen concentration saturation, and $[DO]^0$

204   represents the initial dissolved oxygen concentration, both expressed as mM.

205

206   *Table 1* provides the data given by Cabrera Reina et al. (2012) used in this study:

207   • the values of the initial concentrations for each component ($[C_i]^0$);

208   • the volume of the reactor (V);

209   • the gas–liquid mass transfer coefficient (K_{La}),

210   • the fitted parameters, such as the kinetic constants (k1 to k9) in the reaction rates (r1 to r9);

211   and the stoichiometric coefficients (g1$_{DO}$, g2$_{DO}$, c1$_{DO}$) in the oxygen balance.

212   Regarding the values of initial and saturation dissolved oxygen concentrations

213   ($[DO]^0$and $[DO]^*$), both were set to 0.21 mM.

214

215

216   **Table.1** Kinetic constants, stoichiometric coefficients and initial concentrations values (by

217   Cabrera Reina et al. (2012).

218

219   Furthermore, for the sake of simplicity, nomenclature is completed with the following terms:

220   • Generic reaction time t and final time τ for the reaction (and the ODEs integration), at which

221   the reaction performance is evaluated.

222   • Conversion, $\chi(t)$ and $\chi(\tau)$, which is defined by the following equation and assesses the

223   relative ratio of TOC reduction at a given time:

$$\chi(t) = \left([TOC]^0 - [TOC]^t\right) / [TOC]^0 \qquad (11)$$

224

225

226 • Total amount of H$_2$O$_2$, $A(t)$ and $A(\tau)$, which is defined by the following equation and

227 assesses the total expenditure of H$_2$O$_2$ in the batch run, given by the initial amount and the

228 dosed amount:

$$A(t) = A^0 + C \int_0^t F(\xi)d\xi \quad (mmol) \tag{12}$$

229

230 **2.3 DYNAMIC SIMULATION**

231

232 Based on such kinetic and reactor models, and data, the dynamic simulation of the photo-

233 Fenton process was carried out for a preliminary study of the behaviour of the system. It

234 highlights the advantages of conveniently managing hydrogen peroxide dosage and

235 consequently, the potential benefits arising from further investigation on photo-Fenton

236 optimisation strategies.

237 First, a series of dynamic simulations of pure batch runs (no H$_2$O$_2$ dosage) was performed for

238 the different contaminant loads using different values of the initial concentration of H$_2$O$_2$. The

239 purpose was to investigate the system response to a gradual increase in [TOC]^0 and [H$_2$O$_2$]^0

240 and to identify the saturation threshold from which inefficient reactions boost and TOC

241 conversion, $\chi(\tau)$, drops.

242

243

244 Moreover, four different case studies were also investigated and compared. Especially, a batch

245 case study was selected as reference in order to highlight the benefits arising by performing a

246 reactant dosage. The latter was analysed by simulating three further fed-batch case studies,

247 considering different H$_2$O$_2$ dosage profiles (continuous or stepwise profiles) for different A(t) and

248 for the same A^0=0.

249

250   The *JModelica.org open source platform* [Åkesson et al. (2010)] was selected as the tool to

251   perform the dynamic simulation of the system under study. The simulation environment uses

252   *Assimulo* that is a standalone *Python package* for solving ordinary differential equations (ODEs)

253   and differential algebraic equations (DAEs). Among the different supported solvers, we selected

254   the *CVode solver* to run the dynamic simulation. The CVode [Åkesson et al. (2010)] is a

255   variable-order, variable-step, multi-step algorithm for solving ordinary differential equations of the

256   form:

257

$$\frac{dy}{dt} = \mathrm{f}(t, y), \quad y(t_0) = y_0 \tag{13}$$

258

259   It includes the Backward Differentiation Formulas (BDFs), suitable for stiff problems, but also the

260   Adams-Moulton formulas for non-stiff systems.

261

262

263   **2.4 DYNAMIC OPTIMISATION**

264

265   Subsequently, the dynamic optimisation of the fed-batch photo-Fenton system was carried out.

266   The first step was the optimisation study focused on the following partial objectives:

267

268   ▪   Maximization of the final TOC degradation, $\chi(\tau)$, for a given total amount of H_2O_2 to

269   be dosed, $A(\tau)$, and a fixed final reaction time (τ);

270   ▪   Minimization of $A(\tau)$ to attain a fixed $\chi(\tau)$ within a given τ.

271

272   This study can be used as a sort of sensitivity analysis. Indeed, first $A(\tau)$ and (τ), and then $\chi(\tau)$

273   and (τ) were changed systematically to assess their effect on the final outcome, $\chi(\tau)$ and $A(\tau)$

274   respectively. In this way, as in the case of a traditional sensitivity analysis, the identification of

275   critical factors is possible and it attempts to predict alternative outcomes of the same course of

276   action.

277

278   Finally, the above described partial objectives were gathered in a single objective function

279   proposed in order to perform a more complex optimisation study aiming at finding the optimal

280   H_2O_2 dosage profile, F(t), and reaction time, τ that ensure the minimum processing cost while

281   satisfying operational and environmental constraints.

282

283   The dynamic optimisation problem includes the definition of the system to be optimized, a cost

284   function (the so-called objective function), a set of constraints (equality and inequality path

285   constraints, equality and inequality end-point constraints) and controlled variables. It can be

286   stated in the following general form [Biegler et al. (2007)]:

287

288

$$\min_{z(t),\, u(t),\, p} \varphi\left(z(\tau)\right) \tag{14}$$

$$\text{s.t.}\ \frac{dz(t)}{dt} = \ f(z(t), y(t), u(t), p), \qquad z(t_0) = z_0 \tag{15}$$

$$g(z(t), y(t), u(t), p) = 0 \tag{16}$$

$$g\big(z(t)\big) = 0 \tag{17}$$

$$g(z(\tau), y(\tau), u(\tau), p) \le 0 \tag{18}$$

$$g\big(z(\tau)\big) \le 0 \tag{19}$$

$$y_L \le y(t) \le y_U \tag{20}$$

$$u_L \le u(t) \le u_U \tag{21}$$

$$z_L \le z(t) \le z_U \tag{22}$$

289

290

291   Where $z(t)$ are the differential state variables, $u(t)$ are the control variables, and $y(t)$ are the

292   algebraic variables, all functions of the time $t \in [t_0, \tau]$, while p represents time-independent

293   parameters.

294   In such problem $z(t), u(t),\ y(t)$ and p represent the decision variables, while the constraints are

295   represented by the Differential and Algebraic Equations (DAEs) system, given by *Eqs. (15) -*

296   *(19).* Particularly, Eqs. (16) - (17) and *Eqs. (18) - (19),* represent equality and inequality path

297   and end-point constraints, respectively. Finally, *Eqs. (20) - (22)* define lower and upper bounds

298   for algebraic, control and differential state variables, respectively.

299

300   Currently, dynamic optimisation problems can be solved by using an indirect approach, based

301   on the first order necessary conditions for optimality obtained from Pontryagin's Maximum

302   Principle, and a direct approach based on various strategies that apply non-linear programming

303   (NLP) solvers to the Ordinary Differential Equations (ODEs) or Differential Algebraic Equations

304   (DAEs) model [Biegler et al. (2007); Nocedal et al. (2006)].

305

306   A direct approach, namely direct simultaneous optimisation method, was applied for solving the

307   dynamic optimisation problem. This method is based on orthogonal collocation on finite

308   elements (a fully implicit Runge-Kutta method), and relies on the discretization of both control

309   and state variables by polynomials, whose coefficients become the decision variables of a very

310   large-scale NLP problem.

311

312   The dynamic optimisation problem under study was solved by using the same tool adopted to

313   run the dynamic simulation, or rather, the *JModelica.org open source platform* [Åkesson et al.

314   (2010)]. The *CasADi algorithm* based on direct collocation and implemented in *Python* was

315   used for computing function derivatives and *IPOPT* (Interior Point Optimizer) solver was used

316   for solving the resulting NLP problem.

317

318   ### 2.4.1   *Optimisation study based on partial objectives*

319

320   First, the aim of the dynamic optimisation was to study the interaction between $A(\tau)$ and τ. Such

321   interaction affects the process performance, or rather the final TOC removal, $\chi(\tau)$.

322   Hence, an overview of the best operating conditions to achieve a predetermined $\chi(\tau)$ was

323   provided, as a tool aiding decision-making.

324

325   Concerning the photo-Fenton process, a particular trade-off appears. Adding all hydrogen

326   peroxide at once (no dosage) results in the need of extra hydrogen peroxide (due to inefficient

327   side reactions), which increases the cost of raw materials. Conversely, a slow gradual dosage

328   of a minimum amount of hydrogen peroxide results in an increase of time, which increases

329   operational costs (energy, etc.).

330

331   This poses a Multi-Objective Optimisation (MO) problem. A MO problem can be formulated as a

332   decision-making problem of simultaneous optimisations of two or more objectives that are

333   conflicting in nature (such as the economic cost of a treatment and desired environmental

334   effect). It can be solved by minimizing an objective function subject to some constraints, and the

335   solution is called Pareto optimal, or a Pareto solution ("A Pareto solution is one for which any

336   improvement in one objective can only take place if at least one other objective worsens";

337   [Messac et al. (2003), Pareto (1906)]). The set of Pareto solutions, obtained by systematically

338   varying the constraints to which the objective function is subjected to, is known with the name of

339   Pareto frontier.

340

341   Hence, by building Pareto frontiers, by systematically vary $A(\tau)$ and (τ), and then $\chi(\tau)$ and (τ)

342   to determine their effect on $\chi(\tau)$ and $A(\tau)$ respectively, several optimal operating conditions for

343   different treatment configurations can be easily and quickly identified.

344

345   **Table.2** Scenarios selected to perform the preliminary sensitivity analysis of the fed-batch

346   photo-Fenton system (H_2O_2 dosage)

347

348   Two scenarios (*see Table.2*), all searching for the optimal H_2O_2 dosage profile, F(t), including

349   the starting concentration, $[H_2O_2]^0$ (mM), were investigated and Pareto frontiers were built.

350

351   In *scenario* A, the objective function to be maximized was the outcome, $\chi(\tau)$, subject to a

352   maximum reaction time, τ (h), and the total amount of H_2O_2, to be dosed, $A(\tau)$. In *scenario B*,

353   the objective function to be minimized was $A(\tau)$ subject to a given maximum reaction time and a

354   minimum outcome.

355

356

357   *2.4.2 Optimisation under economic and environmental considerations*

358

359   A final problem was to determine both the addition profile of hydrogen peroxide, F(t), and the

360   reaction time τ that maximize the global performance of the photo-Fenton treatment. This also

361   poses a dynamic optimisation problem that turns into a Multi-Objective Problem when

362   economic, environmental, and operational issues are simultaneously considered.

363

364   The decision variables were:

365   • the reaction time, τ (h),

366   • the initial concentration of hydrogen peroxide, $[H_2O_2]^0$ (mM), and

367   • the dosage profile of hydrogen peroxide, $F(t)$ (L h^{-1}).

368   The constraints are given by the reactor model described in *Eqs. (1) – (10).*

369

370   The problem was addressed by formulating a single objective function φ, representing the total

371   cost (€) to be minimized (*see Eq. 23*). The proposed objective function accounts for the cost of

372   hydrogen peroxide, the operational cost, and the environmental cost that results from an

373   incomplete organic matter degradation. It includes the unit cost coefficients C_1 (€ mmol^{-1}), C_2 (€

374   h^{-1}) and C_3 (€ mmol^{-1}).

375

$$\varphi = C_1 \cdot A(\tau) + C_2 \cdot \tau + C_3 \cdot V(\tau) \cdot \chi(\tau) \cdot [TOC]^0 \qquad (23)$$

376   The coefficient for the cost of the reactant, C_1, was estimated according to current industrial

377   prices. Conversely, different values of C_2 and C_3 were tested in order to elucidate and discuss

378   the trade-off that arises from different operational and environmental costs.

379

380

381   **3.   RESULTS AND DISCUSSION**

382

383   **3.1 Dynamic simulation results**

384

385   Simulation results in terms of $\chi(\tau)$ for different contaminant loads, $[TOC]^0$, and different initial

386   concentrations of hydrogen peroxide, $[H_2O_2]^0$, are presented in *Fig. 3(a)* for a fixed reaction time

387    $\tau = 2h$. Final TOC reduction, $\chi(\tau)$, rises as the initial concentration of H_2O_2 increases, until a

388   threshold saturation value is reached, and then $\chi(\tau)$ drops asymptotically. These results are

389   coherent with the experience and the kinetic model and show that too high hydrogen peroxide

390   concentration can revert the process efficiency by increasing the R concentration, which in turn

391   favours the reaction rate of the inefficient second order reactions.

392

393   The study also shows that by increasing the contaminant load, the peak value of $\chi(\tau)$ reduces

394   from a maximum value of about 85% (for $[TOC]^0$ = 2.085 mM) to a minimum value of about 20%

395   (for $[TOC]^0$ = 33.32 mM). This behaviour is due to the Fe^{2+}/ H_2O_2 ratio, that shows to be

396   ineffective for high values of $[TOC]^0$ (in all previous cases a value of $[Fe^{2+}]^0$ =0.14 mM was set) .

397   This result was then confirmed by running a new simulation for the case of $[TOC]^0$ = 33.32 mM

398   but with an increased value of $[Fe^{2+}]^0$ (set equal to 0.28 mM). Results presented in *Fig. 3 (b)*

399   show that a maximum $\chi(\tau)$ of about 76% can be attained for an initial value of hydrogen

400   peroxide of 120 mM, so increasing by more than 50% the final conversion.

401

402   For the pure batch operation (no dosage after t=0) three main conclusions arise:

403   •   on one hand, given $[TOC]^0$ and $[Fe^{2+}]^0$, an optimum value for the initial concentration of

404   hydrogen peroxide, $[H_2O_2]^0$, exists;

405   •   on the other hand, such optimum value for $[H_2O_2]^0$ may be insufficient to attain complete

406   mineralization ($\chi(\tau)$ = 100%), which indicates that an extra amount of hydrogen peroxide

407   should be subsequently added;

408   •   finally, the amount of iron, $[Fe^{2+}]^0$, confirms to also have a relevant role in the process

409   efficiency and suggests that further work should address the simultaneous optimisation of

410   Fe^{2+} and H_2O_2 dosage.

411

412

413   **Fig.3** Dynamic simulations of pure batch runs (no H_2O_2 dosage) were performed for:

414   (a) Different paracetamol loads (corresponding to $[TOC]^0$=2.085, 4.165, 8.33, 16.66 and 33.32

415   mM), different values of the initial concentration of hydrogen peroxide (in a range between 0

416   and 1000 mM), and for $[Fe^{2+}]^0$=0.14 mM.

417   (b) A given paracetamol load (corresponding to $[TOC]^0$=33.32 mM) and $[Fe^{2+}]^0$=0.28 mM.

418   Final TOC reduction, $\chi(\tau)$, obtained for $\tau = 2h$ is represented for both cases

419

420

421

422   Conversely, *Fig. 4 (a) - (b) - (c) - (d)* show H_2O_2, DO, and TOC simulated concentration profiles

423   for four different case studies (one batch and three fed-batch case studies) that are next

424   discussed. It should be noted that while [DO] is plotted on the secondary axis, the dosage

425   profile is just qualitatively represented without referring it to any units of measurement. In this

426   way, it is easier to observe the different trends between the various investigated case studies,

427   which are detailed below:

428

429   • *Case study A*: a batch case study with no H_2O_2 dosage and 6h reaction time. The total

430   amount of H_2O_2 ($A(\tau) = 158.85$ mmol) was added at the beginning of the process (t=0).

431   It is the reference scenario and it is useful to compare and analyse results in terms of

432   reactant dosage and process efficiency improvement.

433   • *Case study B*: a fed-batch case study, for which the same total amount of H_2O_2 set for

434   the previous case study A ($A(\tau) = 158.85$ mmol) is continuously dosed during the same

435   6h reaction time ($f_{H_2O_2}$(t)=26.48 mmol/h);

436   • *Case study C*: a fed-batch case study, for which half of the same total amount of H_2O_2

437   set for the previous case study B ($A(\tau)$ =79.43 mmol) is continuously released during

438   the first 3h of the total reaction time of 6h ($f_{H_2O_2}$ (t)=26.48 mmol/h);

439   • *Case study D* a fed-batch case study, for which half of the same total amount of H_2O_2

440   set for the case study B ($A(\tau)$ =79.43 mmol) is continuously released during the whole

441   reaction time of 6h ($f_{H_2O_2}$ (t)=13.24 mmol/h).

442   In all cases, 33% v/w ($[H_2O_2]^0$= 35.3 ÷17.65 mM) hydrogen peroxide solution was used for the

443   dosage.

444

445

446   **Fig.4** Comparison of four different dynamic simulation case studies (τ =6h):

447   (a) Pure batch system (no H_2O_2 dosage); 158.85 mmol of H_2O_2 are added all at once ($[H_2O_2]^0_=$

448   35.3 mM); (b) the same total amount of H_2O_2 (158.85 mmol) is continuously dosed until the end;

449   (c) half the amount of H_2O_2 (79.43 mmol) is continuously dosed during half of the time (3h); (d)

450   half the amount of H_2O_2 (79.43 mmol) is continuously dosed during the whole time (6h)

451

452

453   *Fig.4 (a)* presents the results for the case study A and reveals a peak in the DO concentration at

454   1.2h. The increase in the DO concentration is caused by the inefficient reactions promoted by

455   the excess of free radicals R, due to the excess in H_2O_2 concentration. Concerning the H_2O_2

456   concentration trend, it is possible to observe a steep decrease that leads to its consumption in

457   about 3h. It is also important to notice that once the H_2O_2 concentration reaches its minimum

458   value (at 3h), the TOC profile becomes steady and reaches a final value of about 85%.

459

460   Results in *Fig.4 (b)* correspond to the case study B. In this case, after a first gradual and slight

461   increase (about 2 hours), H_2O_2 concentration reaches a maximum value (about 5 mM) and then

462   it remains almost constant for the rest of the time. A different and lower [DO] profile can be

463   observed, compared to case study A. This result suggests that a more effective use of the

464   oxidant has been attained but no significant improvement in the final TOC removal could be

465   observed. Then, DO concentration reaches a maximum value (of about 1.2 mM) at a reaction

466   time of about 3h and starting from this point, it remains constant for the whole process. This

467   suggests that the continuous dosage for the whole reaction time of 6h, cannot be selected as

468   the more effective option.

469

470   *Fig.4 (c)* shows the results for the case study C. The H_2O_2 concentration profile has a similar

471   trend compared to the previous case study B. The [DO] profile, presents also a peak but lower

472   and later compared with the previous case studies (about 0.85 mM and 3.2h, after the end of

473   the dosage, which reveals the inertia of the system). However, half the amount of H_2O_2

474 produces a lower performance (lower final TOC removal) compared with case studies A and B.

475

476 Finally, the results of the last case study are presented in *Fig.4 (d).* A lower H_2O_2 concentration

477 profile can be observed due to the selection of a lower initial concentration value. Also in this

478 case, no significant improvement can be reached in the final TOC removal, although the [DO]

479 profile shows an efficient use of the (insufficient) amount of hydrogen peroxide used (a lower

480 peak that is reached with a significant delay).

481

482 Consequently, the H_2O_2 dosage profile is shown to affect the process performance since it

483 generates different [DO] profiles (in terms of peak and delay) that reveal the extent of inefficient

484 reactions. Furthermore, the simulation of two extreme situations such as case studies A and D

485 reveal existence of an optimum dosage profile attaining the oxidation target with the most

486 efficient use of the oxidant. Hence, a model-based optimisation approach is required in order to

487 propose a systematic methodology allowing the determination of the optimal H_2O_2 dosage

488 maximizing the process efficiency of any contaminant load.

489 In this regard, the sensitivity analysis was a key point of the present work and relevant

490 considerations can be drawn concerning the more effective way to select the hydrogen peroxide

491 dosage profile to gain a certain TOC reduction $\chi(\tau)$ for a specific reaction time τ.

492

493 **3.2 Dynamic optimisation results: optimisation study based on partial objectives**

494

495 The subsequent step is to address the single dynamic optimisation problem by releasing the

496 dosage profile, F(t), as a control variable and defining a specific objective function to be

497 maximized and a specific set of constraints. The solution is implemented using the

498 JModelica.org open source platform [Åkesson et al. (2010)] coupled with Python.

499

500 Two scenarios, scenario A and B in *Table.2*, were discussed. For scenario A the objective

501 function is the final TOC reduction ($\chi(\tau)$), which needs to be the maximized, while the

502 constraints are the reaction time (τ) and the total amount of H_2O_2 ($A(\tau)$) available. Conversely,

503 for scenario B, the objective function is $A(\tau)$, which needs to be to minimized, while the

504   constraints are τ and $\chi(\tau)$. In both cases, the control variable is the flow-rate of hydrogen

505   peroxide solution, F(t), that is dosed during the reaction time, τ . Thus, the optimisation

506   procedure gives the optimal F(t) (inlet flow-rate at each time interval). It also gives the maximum

507   value of TOC reduction and of the minimum total amount of H_2O_2 (objective function values for

508   scenario A and B, respectively) for the specific values selected for the constraints (τ and $A(\tau)$, in

509   the case of scenario A, τ and $\chi(\tau)$ in the case of scenario B) of the problem.

510

511   An advantage of the proposed optimisation strategy is the computer-aided identification of

512   operational opportunities. Therefore, reported experimental results are next compared with the

513   optimal solutions determined under the same conditions. According to [Cabrera Reina et al.

514   (2012)], by adding the total amount of H_2O_2 all at once ($[H_2O_2]^0$=35.3 mM, which corresponds to

515   18 mL total volume of H_2O_2 30% and 8823 mmol) and setting $[Fe^{2+}]^0$=0.14, $[TOC]^0$=8.33 mM,

516   and I=32 W m^{-2}, a final TOC removal of about 60% was attained after 2h of reaction. First, this

517   situation was simulated (*see Fig. 5 (a)*) and a final TOC removal of about 70% was attained,

518   hence experimental results were reproduced within a 10%. Next, assuming the minimization of

519   the total amount of hydrogen peroxide, $A(\tau)$, under the same fixed conditions and variable

520   dosage (scenario B), an optimal dosage profile was determined. In this case, as illustrated in

521   *Fig*.5 (b) and (c), the same final TOC removal of about 60% was attained after 2h, as imposed,

522   but using 14.73 mL of H_2O_2 (corresponding to a total amount of 130 mmol of hydrogen peroxide

523   30%) instead of 18 mL. This is a reduction of more than 18% of the H_2O_2 consumption; this may

524   imply a similar cost reduction that is worth to consider. Furthermore, the optimal H_2O_2 profile at

525   each instant time was also obtained, which could be useful in a perspective of process

526   automatization.

527

528

529

530   **Fig. 5** Optimisation study: comparison between the optimal solution obtained with the proposed

531   optimisation strategy and the experimental results by Cabrera Reina et al. (2012):

532   (a) TOC, H_2O_2, DO concentration profiles obtained by the dynamic simulation of the system

533   under study in the case of $[Fe^{2+}]^0$=0.14, $[H_2O_2]^0$=35.33, $[TOC]^0$=8.33 mM, I=32 W m^{-2} and τ

534   =2h.

535   (b) TOC, H_2O_2, DO concentration profiles obtained for the single optimisation problem aiming at

536   the minimization of the total amount of H_2O_2 in the case of $[Fe^{2+}]^0$=0.14, $[TOC]^0$=8.33 mM, I=32

537   W m^{-2} and τ =2h.

538   (c) F(t) and A(t) obtained by solving the dynamic optmisation problem described in item b)

539

540   Once the optimization procedures have been developed and tuned, multiple optimisation

541   problems can be systematically solved for scenarios A and B, by varying the values of the

542   constraints. Hence, Pareto frontiers can be built by plotting the calculated value of the objective

543   function, referred to one of the two constraints of the problem, versus the other constraint.

544

545   Particularly, the following set of constraints was investigated for the two scenarios:

546   • *Scenario A*: values between 0 and 6 hours and a set of values ranging between 0 and

547   200 mmol, were investigated for τ and A(τ), respectively. Pareto frontiers were built by

548   combining for a specific value of τ, the optimal values of the final TOC removal obtained

549   for the different values of A(τ).

550   • *Scenario B:* in this case, values between 0 and 3 hours, and a set of values ranging

551   between 0 and 1, were investigated for τ and $\chi(\tau)$, respectively. Pareto frontiers were

552   built by combining, for a specific value of τ, the optimal values of A(τ),obtained for the

553   different values of the final TOC removal to be achieved.

554

555   It is worth noting that in order to improve convergence, it was necessary to set a specific

556   number of finite elements (n_e) and of collocation points (n_cp) in each element, such as to set

557   specific options for the CasADi and collocation-based optimisation algorithm that differ from the

558   default ones. For both scenarios, these values were set equal to 90 and 1, respectively.

559

560   Results relating to both scenarios are presented in *Fig.6 (a) – (b)*

561

562

563

564   **Fig. 6** Optimisation study based on partial objectives:

565   (a) Scenario A, Pareto frontiers built by representing the optimal values of the final TOC

566   removal resulting from different values of the total amount of H_2O_2 (comprise between 0 and 200

567   mmol) and of the reaction time (between 0 and 6h);

568   (b) Scenario B, Pareto frontiers obtained by plotting the different optimal values of the total

569   amount of hydrogen peroxide, obtained for different values of the final TOC removal (comprise

570   between 0 and 1) and of the reaction time (comprise between 0 and 4h)

571

572   Pareto frontiers in *Fig.6 (a),* show that to achieve a final TOC removal higher than 90%, starting

573   from an initial concentration of TOC equal to 8.33 mM, at least 4h are required and an

574   approximate amount of hydrogen peroxide of 200 mmol (that corresponds to a concentration of

575   44.44 mM) should be used. Besides, it can be noted that, starting from a reaction time of 4h, no

576   significant difference can be detected in the final TOC removal that can be achieved, neither by

577   increasing the total amount of hydrogen peroxide nor by increasing the reaction time. For

578   example, in 4h it's possible to reach a final TOC removal of about 90% with a total amount of

579   H_2O_2 of 150 mmol (that corresponds to a concentration of 33.33 mM). However, for this same

580   value of the total amount of hydrogen peroxide, increasing the reaction time to 5h produces

581   scarce improvement in the TOC objective. Moreover, it's worth noting that, for a fixed reaction

582   time, a greater conversion of TOC can be obtained by increasing the amount of H_2O_2 to be

583   dosed, but only up to a certain threshold value (which, in all the cases, it's a value between 150

584   and 200 mmol), beyond which the conversion does not significantly improve. This is consistent

585   with the kinetics of the process that describes the increasing effect of the inefficient reactions

586   scavenging H_2O_2 and R, caused by the excess of H_2O_2 concentration.

587

588   Following and analysing the results of scenario A, for scenario B the Pareto frontiers were built

589   for a maximum reaction time of 3h, and are shown in *Fig.6 (b).* It can be noticed that, for the

590   same initial concentration of TOC equal to 8.33 mM, in order to reach 80% of TOC removal, a

591   value of the reaction time higher than 2h must be selected, regardless of the total amount of

592   hydrogen peroxide added to the reactor. This is due to the increasing effect of the inefficient

593   reactions scavenging R and H_2O_2, as already observed for the previous scenario A. A maximum

594   final TOC removal of about 80% can be attained only for a reaction time of 2.5 and 3hh and for

595   a total amount of hydrogen peroxide of about 157 and 120 mmol, respectively. Conversely, for a

596   reaction time of 1h, very low TOC removal can be reached (a maximum value of 30% with a

597   total amount of H_2O_2 of about 97 mmol). Hence, as expected, the higher is the reaction time to

598   be set and the lower will be the amount of hydrogen peroxide to be dosed to reach the same

599   value of the final TOC removal.

600

601   The optimisation study provides both qualitative and quantitative results. It provides a more

602   comprehensive understanding of the process, by investigating the interrelations between the

603   main variables that affect the process efficiency. It also allows quantifying the optimal hydrogen

604   peroxide profile, the total amount of hydrogen peroxide to be dosed, and the processing time to

605   achieve a specific final TOC removal. Besides, it plays also an important role in decision-making

606   support. It gives an overview of the best operating conditions for different scenarios: the best

607   combination of total amount of hydrogen peroxide and the processing time to achieve a specific

608   final TOC removal, the best combination of processing time, and final TOC reduction for a

609   specific value of the total amount of hydrogen peroxide.

610

611   For example, once defined the characteristics of the influent to be treated (Chemical Oxygen

612   Demand (COD), Biological Oxygen Demand (BOD), Total Organic Carbon (TOC) concentration,

613   toxicity, etc.) and the purpose of the treatment, the information provided by the proposed

614   optimisation strategy can be used to select the optimal operating conditions. If the photo-Fenton

615   process is needed as pretreatment to increase the biodegradability of the influent by reducing

616   the initial TOC concentration of at least 50% and if the processing time cannot be higher than

617   2h, the optimal amount of hydrogen peroxide required is revealed (*Fig.6 (a)*) to be 100 mmol

618   (corresponding to a concentration of 22.22 mM). The relative optimal hydrogen peroxide dosage

619   during the 2 hours is also provided.

620

621   **3.3 Dynamic optmisation results: optimisation under economic and environmental**

622   **considerations**

623

624   Finally, a different optimisation study was performed by defining an economic objective function

625   (*see Eq. 23*) aimed at determining the addition profile for hydrogen peroxide and the reaction

626   time that optimize the total cost (*Eq.23*) of a fed-batch photo-Fenton process. For this study, the

627   coefficient accounting for the cost of the reactant, C_1, was estimated according to current

628   industrial prices while a specific set of values has been investigated for unit cost coefficients

629   accounting for the operational and environmental costs, namely C_2 and C_3 respectively, and are

630   shown in the following *Table.3*:

631

632

633   **Table.3** Values selected for the unit cost coefficients accounting for H_2O_2, operational and

634   environmental cost, and namely C_1 (€ mmol^{-1}) , C_2 (€ h^{-1}) and C_3 (€ mmol^{-1}), respectively

635

636   Hence, by the combination of the different values set for C_2 and C_3, it was possible to investigate

637   24 different scenarios. For all of them, the number of finite elements (n_e) and the number of

638   collocation points in each element (n_cp) were set to 30 and 1, respectively, in order to improve

639   convergence. The results obtained are presented in *Fig.7 and 8*. In *Fig. 7 (a) – (b)* a clustered

640   column chart allows to highlight the trade-off between the operational and the environmental

641   cost, with respect to the reaction time that must be set and the final TOC removal that must be

642   achieved, respectively.

643

644   As it should be anticipated, when the environmental unit cost coefficient is equal to zero there is

645   no need to apply the photo-Fenton process and so the reaction time and the final TOC removal

646   turn out to be zero, regardless of the value of the operational unit cost coefficient. Conversely,

647   for an operational unit cost coefficient equal to 0 € h^{-1}, the maximum reaction time of 6h and the

648   maximum TOC removal (mineralization) were found out, regardless of the value of the

649   environmental unit cost coefficient (except for the above discussed case with C_3 equal to 0 €

650   mmol^{-1}).

651

652   As expected, for a fixed value of the operational unit cost coefficient, as the environmental unit

653   cost coefficient increases (so becoming more relevant the environmental cost than the

654 operational cost), the reaction time and the TOC reduction increase too. It is worth noting that in

655 the case of an operational unit cost coefficient of 100 and 500 € h^{-1}, by increasing the

656 environmental unit cost coefficient from 0 to 10 € mmol^{-1}, no increase in the reaction time and in

657 TOC removal was recorded. In this case, the reaction time as well as the TOC removal

658 assumed the minimum value (0h and 0% respectively). The same results can be observed in

659 the case of an operational unit cost coefficient equal to 1000 € h^{-1}, regardless of the value of the

660 environmental unit cost coefficient. This is due to the greater relevance of the operational cost

661 compared to the environmental cost. Thus, in these cases, the best solution is to avoid the

662 process. Hence, the greater is the environmental cost the greater is the need for TOC removal

663 and so the longer will be the process. Finally, for a same value of the environmental unit cost

664 coefficient, the increase in the operational unit cost coefficient produces a decrease in the

665 reaction time and in the TOC reduction that can be attained.

666

667

668

669

670

671 **Fig. 7** Economic optimisation study:

672 (a) Clustered column chart representing the reaction time obtained by varying the operational

673 unit cost coefficient (C_2) and the environmental unit cost coefficient (C_3);

674 (b) Clustered column chart representing the final percentage of TOC removal, obtained by

675 varying the operational unit cost coefficient (C_2) and the environmental unit cost coefficient (C_3)

676

677

678

679 Then, a specific case study among the ones above described has been selected in order to

680 analyze the results in terms of cost functions (€), such as environmental, operational, hydrogen

681 peroxide and total cost functions and in terms of total amount of hydrogen peroxide (mmol)

682 added during the processing time.

683 As a significant example, the scenario corresponding to the following values of C_2 and C_3 was

684   selected:

685

686   ▪ $C_2 = 50$ € h^{-1}

687   ▪ $C_3 = 10$ € mmol^{-1}

688

689   These results are presented in *Fig.8*. As can be noticed, the most relevant cost is represented

690   by the environmental cost that influences the total cost function trend. It is important to notice

691   that with the introduction of the environmental cost, the total cost function starts to decrease,

692   due to the TOC reduction and finally tends to a plateau, due to the slower degradation rates

693   characterizing the final steps of the reaction.

694

695   Each of these cost values correspond to the objective function value of the best case for each

696   set of cost coefficients, initial values and constraints, but it also corresponds to the optimal

697   dosage profile that causes these costs. Hence, the optimization study of the model allows

698   identifying the best cost attainable as well as the continuous control action F(t) that allows

699   obtaining it. Thus, for each new situation a new optimization will produce a new optimal dosage

700   profile that will minimize the operational cost (economic and environmental).

701

702

703

704   **Fig.8** Optimisation study based on environmental and economic considerations:

705   Representation of the environmental, operational, hydrogen peroxide and total cost functions,

706   as well as the total amount of hydrogen peroxide added during the processing time obtained by

707   setting an operational unit cost coefficient equal to 50 € h^{-1} and an environmental unit cost

708   coefficient equal to 10 € mmol^{-1}

709

710

711

712

713

714   **4. CONCLUSIONS**

715

716   This work has investigated the efficient photo-catalytic elimination of environmental pollutants

717   such as recalcitrant organic compounds. While many works in the literature report a great deal

718   of experimental data on Advanced Oxidation Processes, fewer works address the modelling of

719   these processes. Yet, models need to be systematically exploited to identify opportunities and

720   determine efficient operation modes for automated processing.

721

722   This work provides a novel simulation and multi-objective optimization framework for taking

723   advantage of available kinetic models. It has been applied to the photo-Fenton process in order

724   to map the trade-offs involved in its efficient management and determine the best operation

725   recipes in the form of optimal hydrogen peroxide dosage profile. Optimal recipes under different

726   operational, economic and environmental constraints have been found out for the batch-wise

727   photo-Fenton treatment of paracetamol solutions.

728

729   In particular, a preliminary dynamic simulation showed that a model-based optimisation

730   approach is important to develop a systematic approach to the selection of a H_2O_2 dosage

731   profile enhancing process efficiency while reducing experimental work. It also evidenced the

732   opportunity to attempt the simultaneous optimization of the Fe^{2+}/H_2O_2 ratio in future works.

733

734   Hence, a subsequent dynamic optimisation strategy was proposed to determine the optimal

735   dosage profile. Next, a series of optimisation runs allowed illustrating the different variables

736   affecting the process efficiency and system behaviour. It was also possible to show the role of

737   the hydrogen peroxide and of the reaction time in the final TOC reduction.

738

739   Especially, for the case study addressed, it was possible to reveal that the only way to reduce

740   TOC beyond 90%, was to set a reaction time higher than 4h and a total amount of H_2O_2

741   comprised between 150 and 200 mmol. The latter range represents a threshold value for the

742   total amount of H_2O_2 that highlights the activation of the inefficient reactions scavenging H_2O_2

743   and free radicals. Conversely, very low TOC reduction can be achieved for a reaction time lower

744   than 1.5h.

745

746   Pareto frontiers have shown to be a tool providing practical process insight and understanding

747   for sensible decision-making. Furthermore, many other response surfaces could be derived

748   from the model in order to facilitate the analysis of the process for different optimisation

749   objectives.

750

751   Finally, an optimisation study accounting for economic as well as environmental factors was

752   presented. A proper objective function was formulated in order to take into consideration the

753   trade-off between the environmental and the operational costs that affects the setting of the

754   reaction time and the final TOC reduction to be achieved. The study highlighted a predictable

755   behaviour of the system addressed, thus confirming the reliability and efficiency of the proposed

756   methodology.

757

758   This work concludes that the availability of a reliable model is necessary for understanding and

759   efficiently operating the photo-Fenton process. Thus, further experimental effort is required

760   towards this end, by fitting models into particular experimental data and validating the proposed

761   optimisation strategy, which will be then used as starting point for future monitoring (soft

762   sensing), control and automation of the photo-Fenton process.

763

764

770

771

772

773

774 **REFERENCES**

775

776 Åkesson J, Årén KE, Gäfvert M, Bergdahl T, Tummescheit H (2010) Modeling and

777 Optimization with Optimica and JModelica.org—Languages and Tools for Solving Large-

778 Scale Dynamic Optimization Problem. Computers and Chemical Engineering.

779

780 Andreozzi R, D'Apuzzo A, Marotta R (2000) A kinetic model for the degradation of

781 benzothiazole by Fe^{3+}-photo-assisted Fenton process in a completely mixed batch reactor.

782 J Hazard Mater B 80: 241-257.

783

784 Biegler LT (2007) An overview of simultaneous strategies for dynamic optimization.

785 Chemical Engineering and Processing 46: 1043–1053.

786

787 Cabrera Reina A, Santos-Juanes L, García JL, Casas JL, Sánchez JS (2012) Modelling

788 photo-Fenton process for organic matter mineralization, hydrogen peroxide consumption

789 and dissolved oxygen evolution. Appl Catal B 119-120: 132-138.

790

791 Conte LO, Farias J, Albizzati ED, Alfano OM (2012) Photo-Fenton Degradation of the

792 Herbicide 2, 4-Dichlorophenoxyacetic Acid in Laboratory and Solar Pilot-Plant Reactors.

793 Ind. Eng. Chem. Res. 51: 4181−4191.

794

795 Farias J, Rossetti GH, Albizzati ED, Alfano OM (2007) Solar Degradation of Formic Acid:

796 Temperature Effects on the Photo-Fenton Reaction. Ind. Eng. Chem. Res. 46: 7580-7586.

797

798 Jeong J, Yoon J (2005) pH effect on OH radical production in photo/ferrioxalate system.

799 WaterResearch 39: 2893–2900.

800

801 Kusic H, Koprivanac N, Loncaric Bozic A, Selanec I, (2006) Photo-assisted Fenton type

802 processes for the degradation of phenol: a kinetic study. J. Hazard. Mater. 136: 632–644.

803

804 Messac A, Ismail-Yahaya A, Mattson CA (2003) The normalized normal constraint method

805 for generating the Pareto frontier. 1 Structural and Multidisciplinary Optimization 25(2): 86–

806 98. doi: 10.1007/s00158-002-0276.

807

808 Miralles-Cuevas S, Audino F, Oller I, Sánchez-Moreno R, Sánchez Pérez JA, Malato S

809 (2014) Pharmaceuticals removal from natural water by nanofiltration combined with

810 advanced tertiary treatments (solar photo-Fenton, photo-Fenton-like Fe(III)–EDDS complex

811 and ozonation). Separation and Purification Technology 122: 515–522.

812

813 Moreno-Benito M, Yamal-Turbay E, Espuña A, Pérez-Moya M, Graells M. (2013) Optimal

814 recipe design for Paracetamol degradation by advanced oxidation processes (AOPs) in a

815 pilot plant . Proceedings of the 23rd European Symposium on Computer Aided Process

816 Engineering – ESCAPE 23, 9 - 12 June, 2013, Lappeenranta, Finland.

817

818 Nocedal J, Wächter A, Waltz RA (2006) Adaptive Barrier Strategies for Nonlinear Interior

819 Methods. Research Report RC 23563, IBM T. J. Watson Research Center, Yorktown, USA.

820

821 Oller I, Malato S, Sánchez-Pérez JA (2011) Combination of Advanced Oxidation Processes

822 and biological treatments for wastewater decontamination—A review. Science of the Total

823 Environment 409: 4141–4166.

824

825 Ortega-Gómez E, Moreno Úbeda JC, Álvarez Hervás JD, Casas López JL, Santos-Juanes

826 Jordá L, Sánchez Pérez JA (2012) Automatic dosage of hydrogen peroxide in solar photo-

827 Fenton plants: Development of a control strategy for efficiency enhancement. Journal of

828 Hazardous Materials 237-238: 223-20.

829

830 Pareto V (1906) Manuale di Economica Politica, Societa Editrice Libraria. Milan; translated

831 into English by A.S. Schwier as Manual of Political Economy.

832

833   Pérez-Moya M, Graells M, Buenestado P, Mansilla HD (2008) A comparative study on the

834   empirical modeling of photo-Fenton treatment process performance. Appl Catal B,

835   Environmental 84: 313–323.

836

837   Pignatello J, Oliveros E, MacKay A (2006) Advanced oxidation processes for organic

838   contaminant destruction based on the Fenton reaction and related chemistry. Crit. Rev.

839   Environ. Sci. Technol. 36:1–84.

840

841   Prieto-Rodríguez L, Oller I, Zapata A, Agüera A, Malato S (2011) Hydrogen peroxide

842   automatic dosing based on dissolved oxygen concentration during solar photo-Fenton.

843   Catalysis Today 161: 247–254.

844

845   Ribeiro AR, Nunes OC, Pereira MFR, Silva AMT (2015) An overview on the advanced

846   oxidation processes applied for the treatment of water pollutants defined in the recently

847   launched Directive 2013/39/EU. Environment International 75: 33–51.

848

849   Yamal-Turbay E, Graells M, Pérez-Moya M (2012) Systematic Assessment of the Influence

850   of Hydrogen Peroxide Dosage on Caffeine Degradation by the Photo-Fenton Process. Ind.

851   Eng. Chem. Res. 51: 4770−4778.

852

853   Yamal-Turbay E, Jaén E, Graells M, Pérez-Moya M (2013) Enhanced photo-Fenton

854   process for tetracycline degradation using efficient hydrogen peroxide dosage. Journal of

855   Photochemistry and Photobiology A Chemistry 267: 11-16.

856

857   Zapata A, Oller I, Rizzo L, Hilgert S, Maldonado MI, Sánchez-Pérez JA, Malato S (2010)

858   Evaluation of operating parameters involved in solar photo-Fenton treatment of wastewater:

859   Interdependence of initial pollutant concentration, temperature and iron concentration. Appl.

860   Catal. B 97: 292–298.

Table.1 Kinetic constants, stoichiometric coefficients and initial concentrations values (by Cabrera Reina et al.2012).

Kinetic constants

k1	k2	k3	k4	k5	k6	k7	k8	k9
$mM^{-1} h^{-1}$	$(W\,m^{-2})^{-1} mM^{-1} h^{-1}$	$mM^{-1} h^{-1}$	$mM^{-1} h^{-1}$	$(mM^{2})^{-1} h^{-1}$	$mM^{-1} h^{-1}$	$mM^{-1} h^{-1}$	$mM^{-1} h^{-1}$	$mM^{-1} h^{-1}$
8.81	5.63	75.8	42798	2643	257	2865	271	107

Stoichiometric coefficients

$g1_{DO}$	$g2_{DO}$	$c1_{DO}$	kla
			h^{-1}
0.75	0.47	0.10	2.7

Initial concentrations

$[Fe^{2+}]^0$	$[Fe^{3+}]^0$	$[H_2O_2]^0$	$[R]^0$	$[M]^0$	$[MX_1]^0$	$[MX_2]^0$	$[DO]^0$	$[TOC]^0$	Total volume V	Irradiance I
mM	mM	mM	mM	mM	mM	mM	mM	mM	L	$W\,m^{-2}$
0.14	0	35.3	0	8.33	0	0	0.21	8.33	4.5	32

Table.2 Scenarios selected to perform the preliminary sensitivity analysis of the fed-batch photo-Fenton system (H_2O_2 dosage)

	Objective Function	Decision variables	Constraints
scenario A	Max $\chi(\tau)$	$F(t)$	τ
		$[H_2O_2]^0$	$A(\tau)$
scenario B	Min $A(\tau)$	$F(t)$	τ
		$[H_2O_2]^0$	$\chi(\tau)$

Table.3 Values selected for the unit cost coefficients accounting for H_2O_2, operational and environmental cost, and namely C_1 (€ mmol^{-1}) , C_2 (€ h^{-1}) and C_3 (€ mmol^{-1}), respectively

C_1	C_2	C_3
€ mmol^{-1}	€ h^{-1}	€ mmol^{-1}
0.0001	0	0
	10	10
	50	50
	100	100
	500	
	1000	
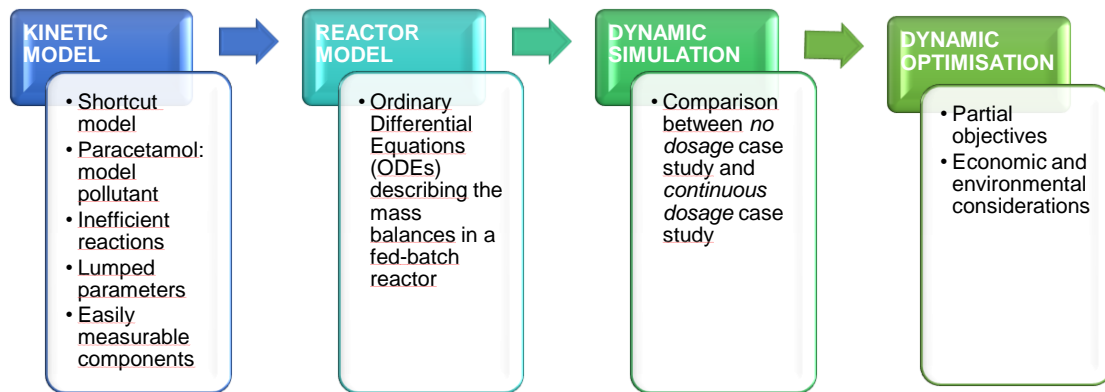
Fig.1 Scheme of the proposed methodology consisting of four specific steps: the kinetic modelling, the reactor modelling, the dynamic simulation and the dynamic optimisation

Figure2
Click here to download Figure: Fig.2.docx

$$Fe^{2+} + H_2O_2 \xrightarrow{1} Fe^{3+} + R \qquad\qquad R + M \qquad\qquad R + M + DO$$

$$Fe^{3+} + hv \xrightarrow{2} Fe^{2+} + R \qquad\qquad R + MX_1 \qquad\qquad$$

$$R + H_2O_2 \qquad R + R \qquad\qquad R + MX_2$$

$$DO$$

$$CO_2$$
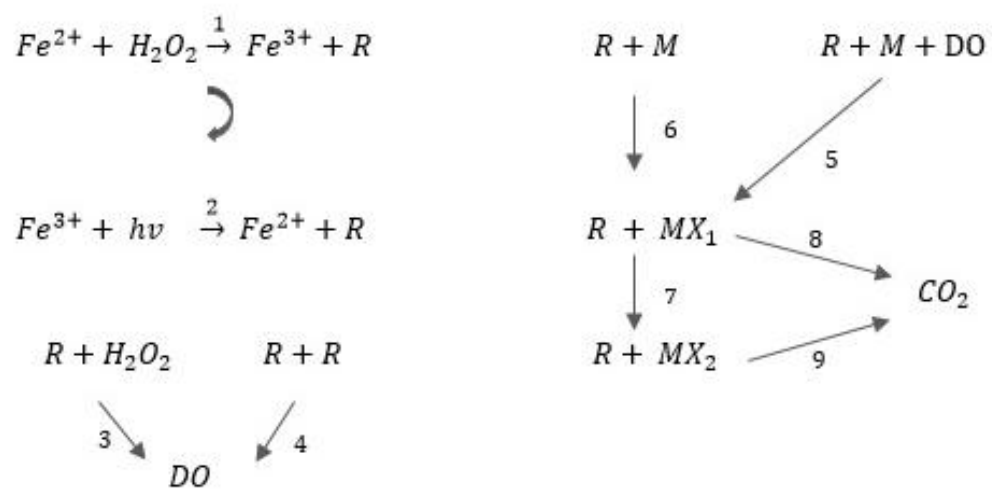
Fig.2 Kinetic mechanism proposed by Cabrera Reina et al. (2012)

Figure3
Click here to download Figure: Fig.3.docx
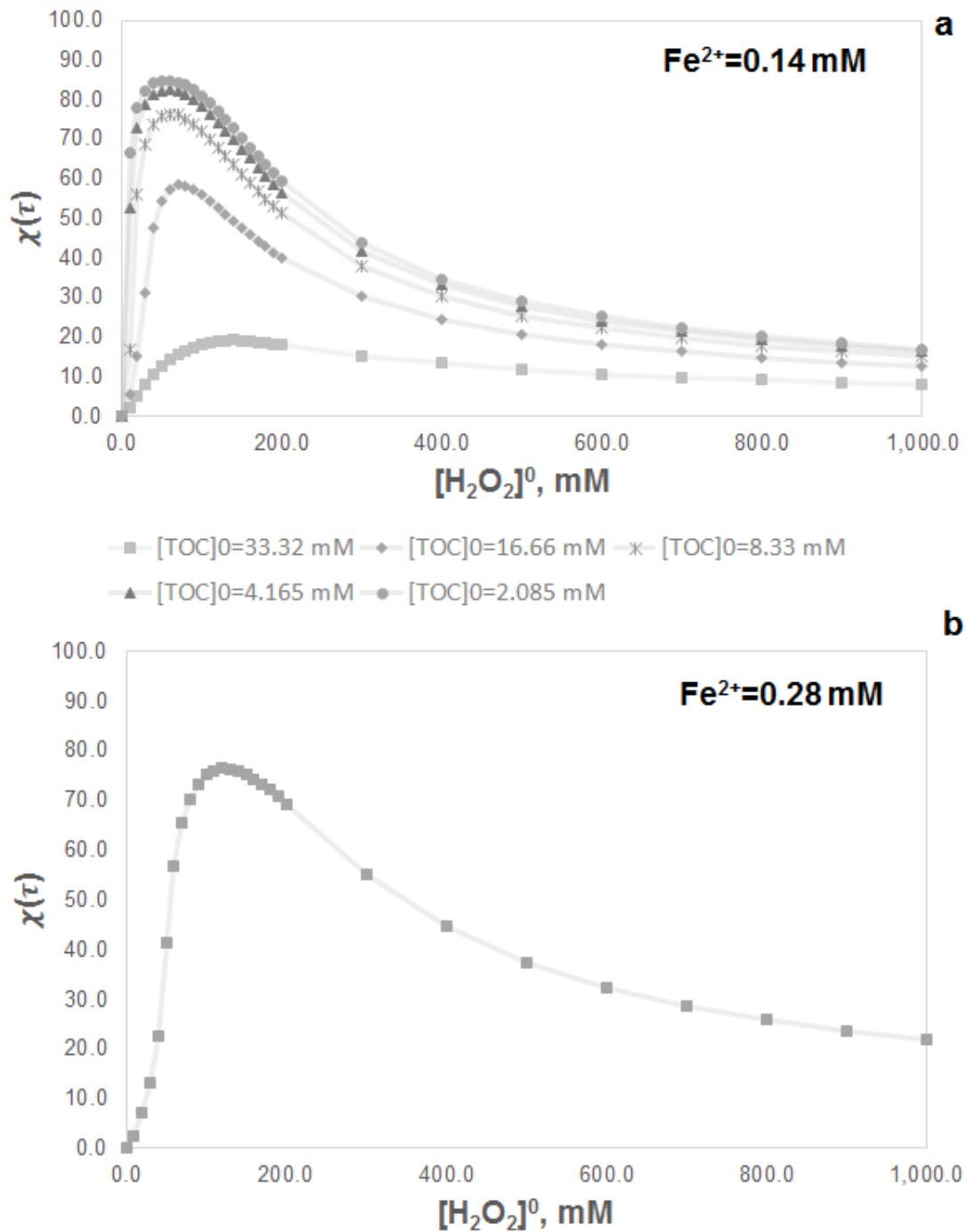
Fig.3 Dynamic simulations of pure batch runs (no H_2O_2 dosage) were performed for:

(a) Different paracetamol loads (corresponding to $[TOC]^0$=2.085, 4.165, 8.33, 16.66 and 33.32 mM), different values of the initial concentration of hydrogen peroxide (in a range between 0 and 1000 mM), and for $[Fe^{2+}]^0$=0.14 mM.

(b) A given paracetamol load (corresponding to $[TOC]^0$=33.32 mM) and $[Fe^{2+}]^0$=0.28 mM.

Final TOC reduction, $\chi(\tau)$, obtained for $\tau = 2h$ is represented for both cases

Figure4
Click here to download Figure: Fig.4.docx
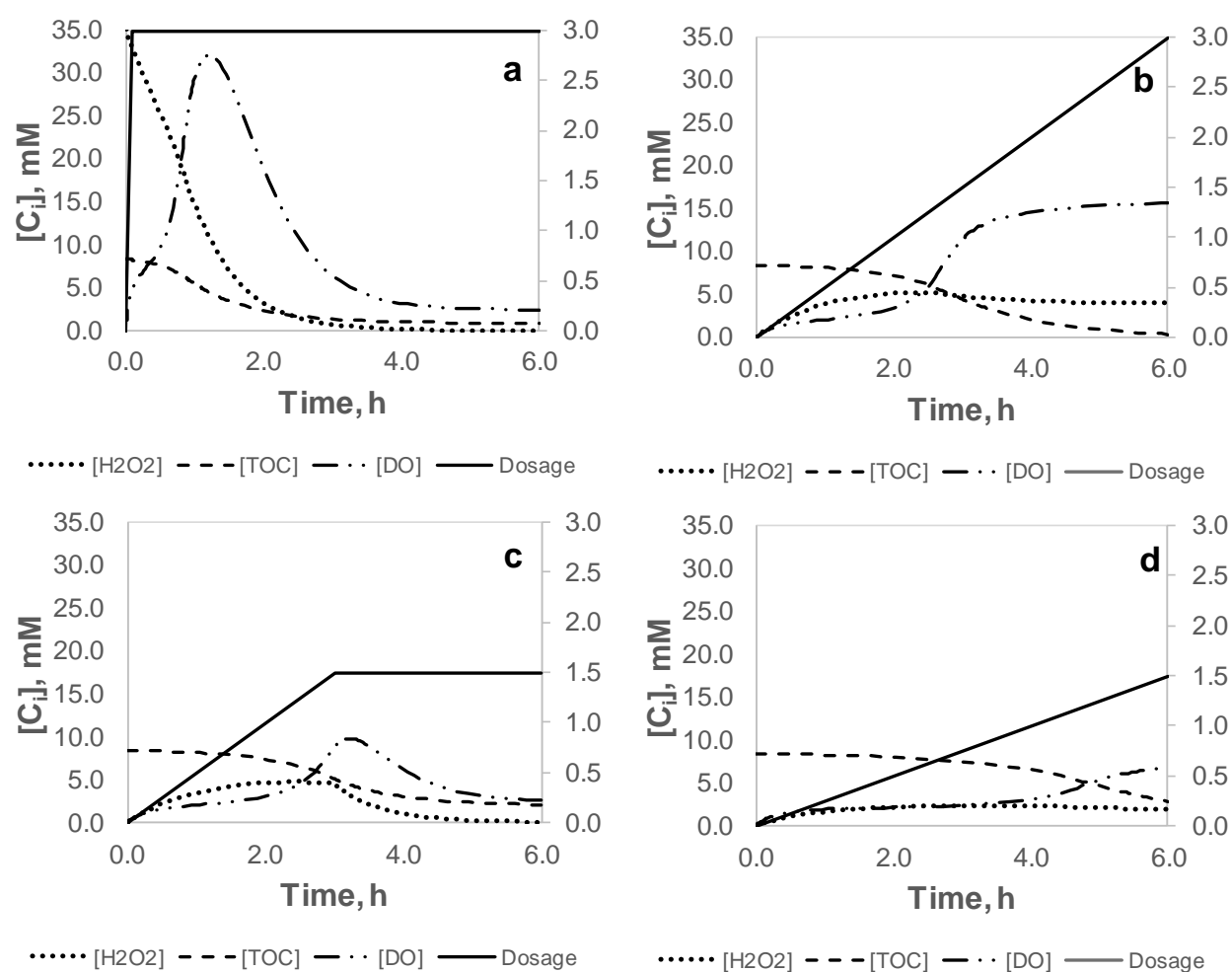
Fig.4 Comparison of four different dynamic simulation case studies (τ =6h):

(a) Pure batch system (no H_2O_2 dosage); 158.85 mmol of H_2O_2 are added all at once ($[H_2O_2]^0$ = 35.3 mM); (b) the same total amount of H_2O_2 (158.85 mmol) is continuously dosed until the end; (c) half the amount of H_2O_2 (79.43 mmol) is continuously dosed during half of the time (3h); (d) half the amount of H_2O_2 (79.43 mmol) is continuously dosed during the whole time (6h)

Figure5
Click here to download Figure: Fig.5.docx
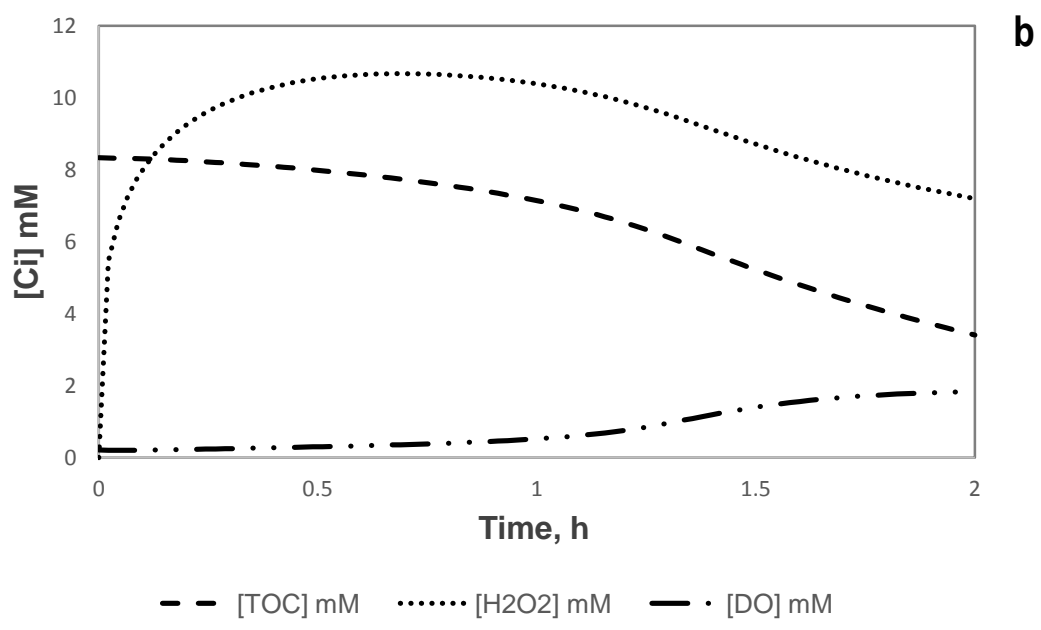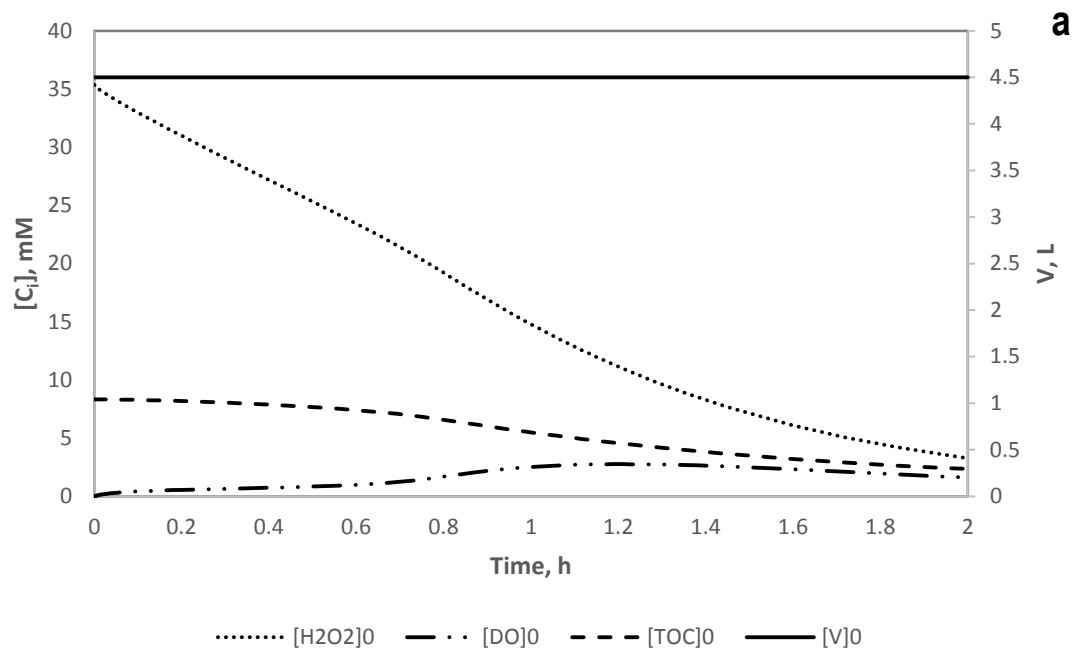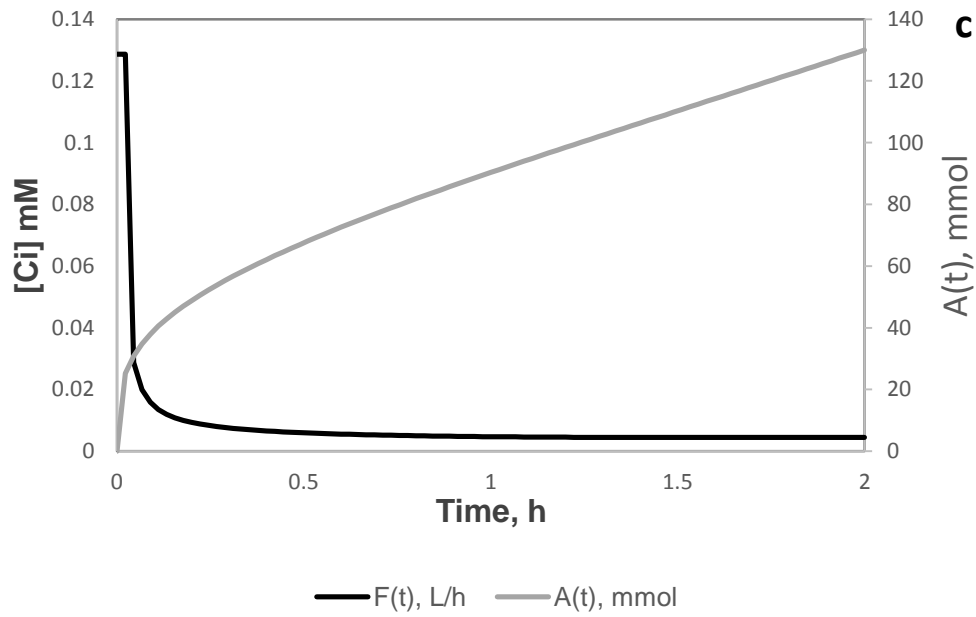
a

Legend: [H2O2]0, [DO]0, [TOC]0, [V]0

b

Legend: [TOC] mM, [H2O2] mM, [DO] mM

Fig. 5 Optimisation study: comparison between the optimal solution obtained with the proposed optimisation strategy and the experimental results by Cabrera Reina et al. (2012):

(a) TOC, H_2O_2, DO concentration profiles obtained by the dynamic simulation of the system under study in the case of $[Fe^{2+}]^0=0.14$, $[H_2O_2]^0=35.33$, $[TOC]^0=8.33$ mM, I=32 W m^{-2} and τ =2h.

(b) TOC, H_2O_2, DO concentration profiles obtained for the single optimisation problem aiming at the minimization of the total amount of H_2O_2 in the case of $[Fe^{2+}]^0=0.14$, $[TOC]^0=8.33$ mM, I=32 W m^{-2} and τ =2h.

(c) F(t) and A(t) obtained by solving the dynamic optmisation problem described in item b)
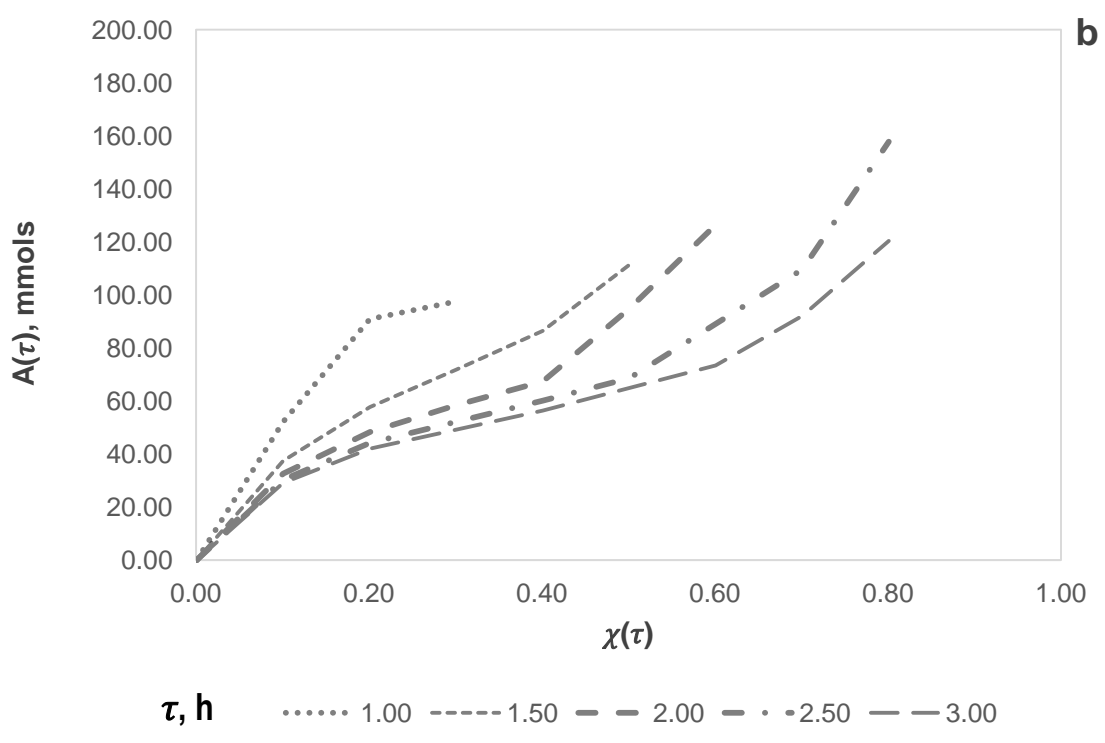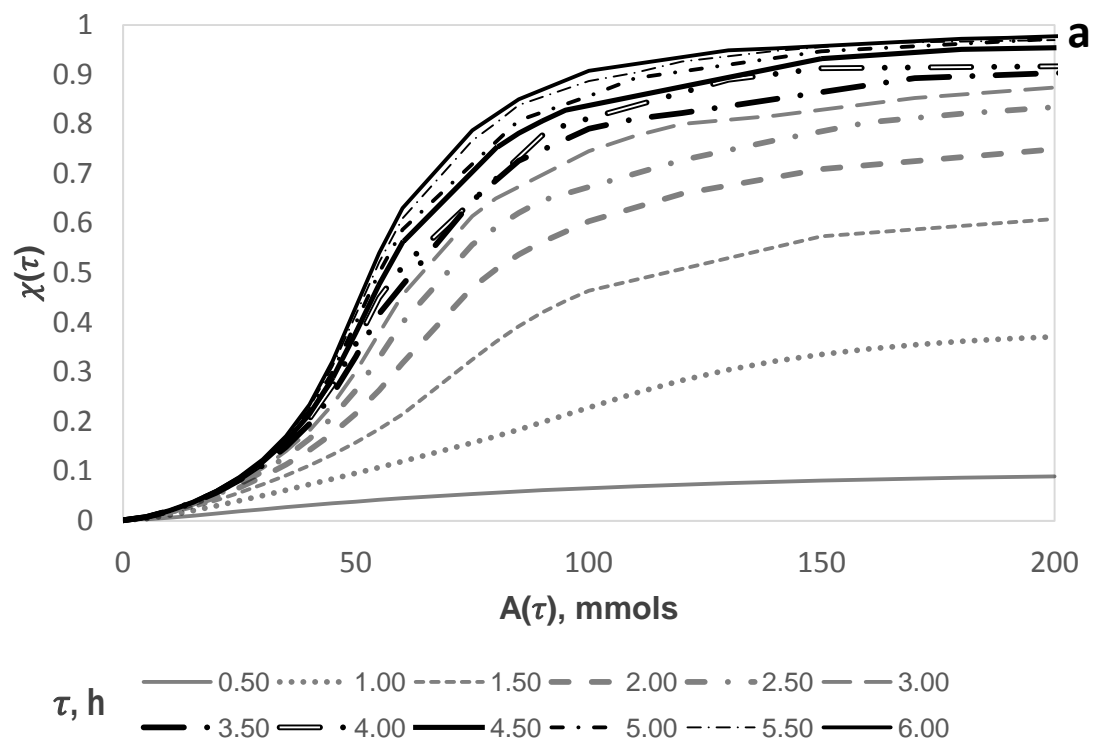
Fig. 6 Optimisation study based on partial objectives:

(a) Scenario A, Pareto frontiers built by representing the optimal values of the final TOC removal resulting from different values of the total amount of H_2O_2 (comprise between 0 and 200 mmol) and of the reaction time (between 0 and 6h);

(b) Scenario B, Pareto frontiers obtained by plotting the different optimal values of the total amount of hydrogen peroxide, obtained for different values of the final TOC removal (comprise between 0 and 1) and of the reaction time (comprise between 0 and 4h)

Figure7
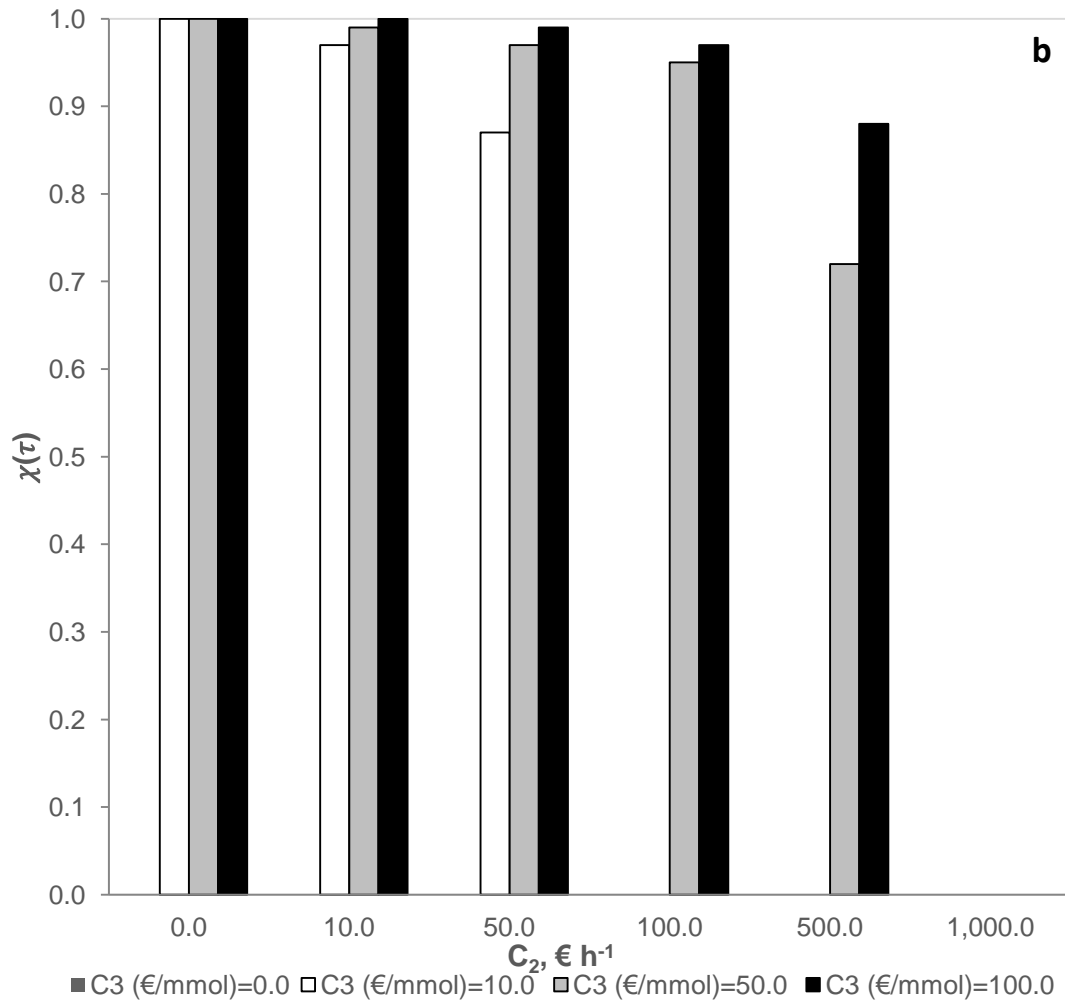**Click here to download Figure: Fig.7.docx**
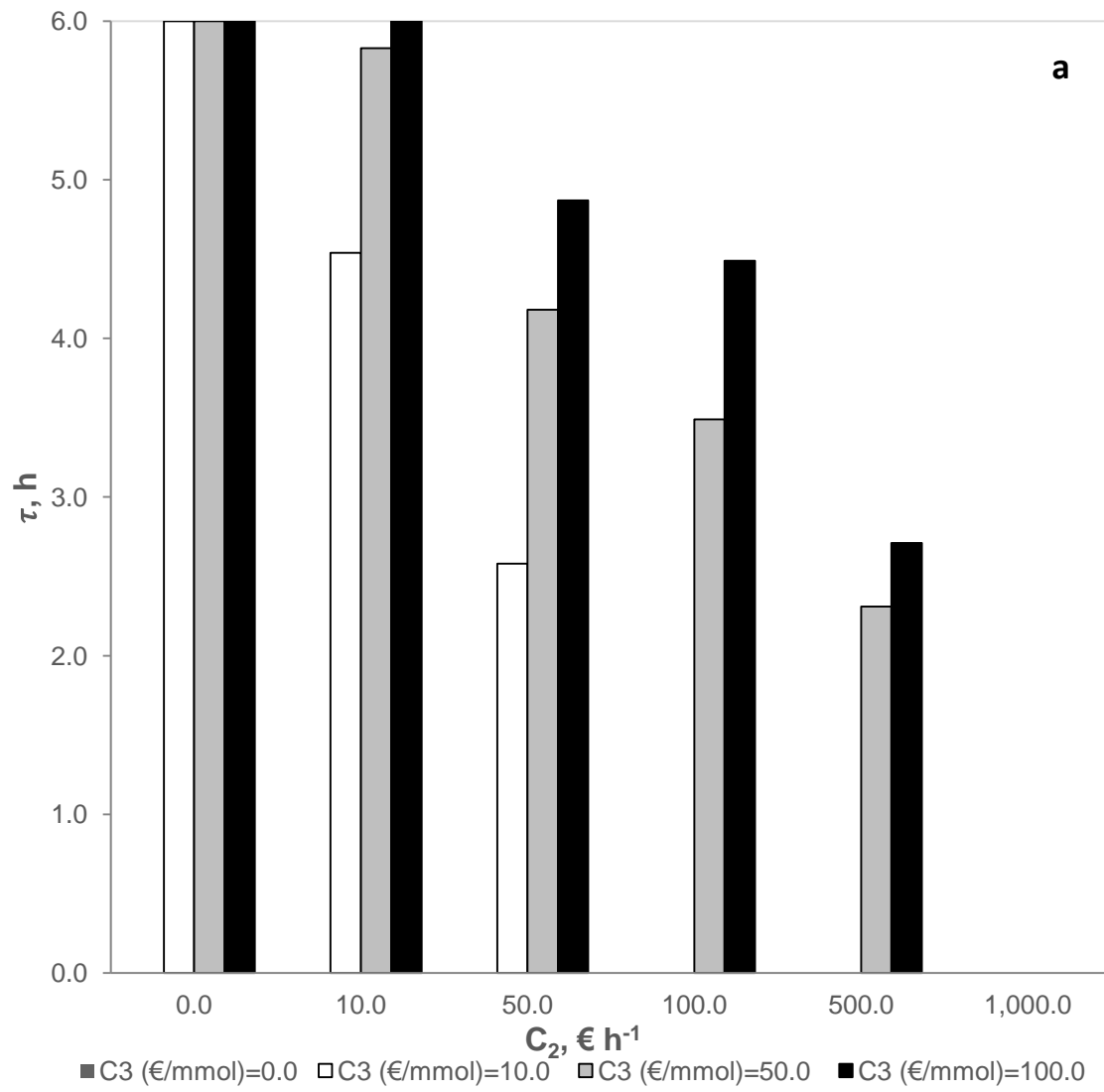
Fig. 7 Economic optimisation study:

(a) Clustered column chart representing the reaction time obtained by varying the operational unit cost coefficient (C_2) and the environmental unit cost coefficient (C_3);

(b) Clustered column chart representing the final percentage of TOC removal, obtained by varying the operational unit cost coefficient (C_2) and the environmental unit cost coefficient (C_3)
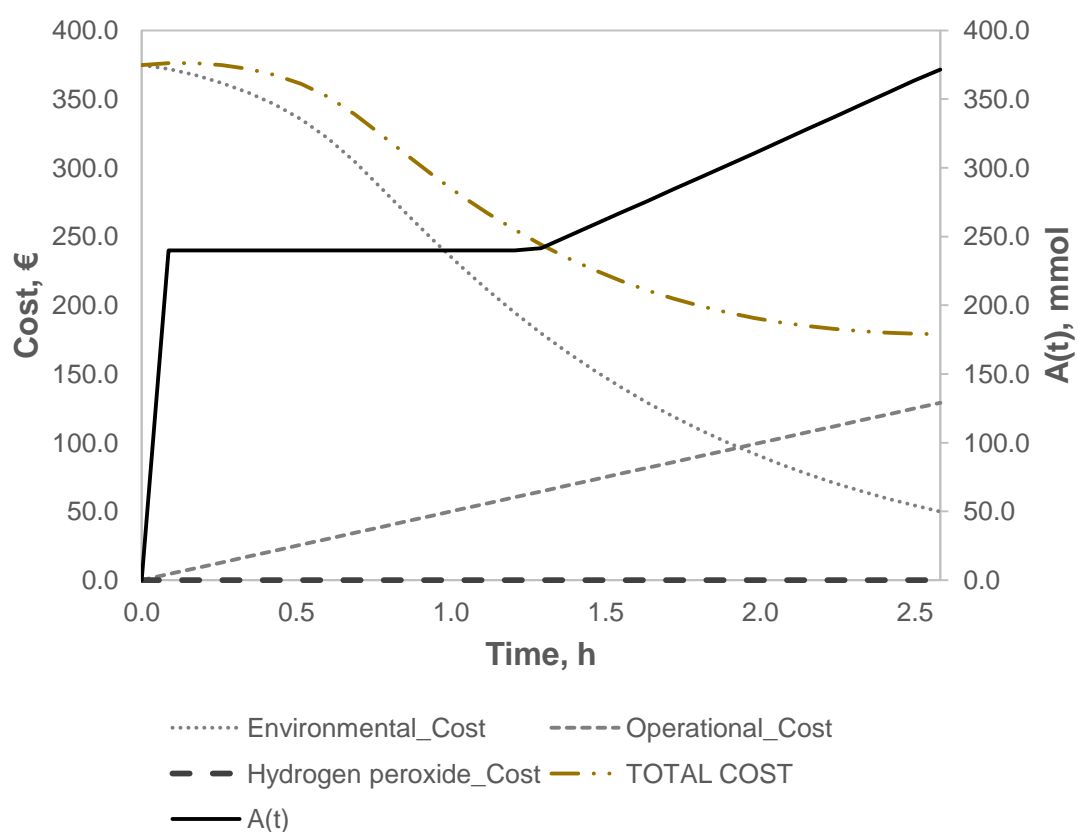
Fig.8 Optimisation study based on environmental and economic considerations: Representation of the environmental, operational, hydrogen peroxide and total cost functions, as well as the total amount of hydrogen peroxide added during the processing time obtained by setting an operational unit cost coefficient equal to 50 € h^{-1} and an environmental unit cost coefficient equal to 10 € $mmol^{-1}$